JOURNAL OF GEOPHYSICAL RESEARCH, VOL. 103, NO. C1, PAGES 1193–1208, JANUARY 15, 1998

Variability in Arctic sea ice optical properties

Donald K. Perovich
U.S. Army Cold Regions Research and Engineering Laboratory, Hanover, New Hampshire

Collin S. Roesler
Department of Marine Sciences, University of Connecticut, Groton

W. Scott Pegau
College of Oceanic and Atmospheric Sciences, Oregon State University, Corvallis

Abstract. The optical properties of sea ice exhibit considerable spatial, temporal, and spectral variability. During a field experiment at Barrow, Alaska, we examined the horizontal variability of spectral albedo and transmittance as well as the vertical variability of in-ice radiance. Temporal changes were monitored under cold conditions in April and during the onset of melt in June. Physical properties, including ice structure and concentrations of particulate and dissolved material, were measured to provide a context for understanding the observed temporal, horizontal, vertical, and spectral variability in optical properties. For snow-covered first-year ice in April, wavelength-integrated (300–3000 nm) albedos were high (0.8) and spatially uniform, but there was considerable variability in transmittance. Transmittance at 440 nm ranged by more than a factor of 2 over horizontal distances of only 25 m, owing primarily to differences in snow depth, although spectral variations in transmittance indicate that absorbing organic materials in the ice column contribute significantly to the horizontal variability. Peak values of transmittance in April were 1% near 500 nm, decreasing at both longer and shorter wavelengths. At the onset of melt in June, the ice surface rapidly evolved into a variegated mixture of melting snow, bare ice, and melt ponds. Albedos were much lower and exhibited considerable spatial variability, ranging from 0.2 to 0.5 over distances of a few meters concomitant with the variation in surface characteristics. Transmission increased over the spring transition as surface characteristics evolved to decrease albedo and as in-ice structure was altered by heating to reduce attenuation within the ice. The exception to this trend occurred over a period of a few days when an algal bloom developed on the underside of the ice and transmission was significantly reduced. Variability in the in-ice spectral radiance values was observed between nearby sites in both first-year and multiyear ice. While the radiance measurements are strongly dependent on the incident solar radiance, under similar solar conditions there was an observed shift in the peak of the maximum in the spectral radiance from 460 nm in clean ice to between 500 and 550 nm in ice that contained particulates in the surface layer. More impressive spectral shifts were found in an old melt pond that had accumulated particles at its base. Not only was there a strong shift in the spectral nature of the radiance as a function of horizontal distance, but there also existed large changes vertically within the ice. The vertical variability in the radiance attenuation coefficient was spatially coherent with variations in both the physical structure of the ice, especially grain size, and the concentrations of particulate and dissolved materials entrapped in the ice. Not surprisingly, the short-lived algal layer on the underside of the ice resulted in changes in the radiance attenuation coefficient from approximately 1 m^{-1} in the interior ice to approximately 40 m^{-1} within that layer.

1. Introduction

The optical properties of sea ice exhibit considerable seasonal, spatial and spectral variability. Temporal changes in optical properties have been observed during the summer melt season [*Grenfell and Maykut*, 1977; *Grenfell and Perovich*, 1984; *Perovich*, 1994] and fall freeze-up [*Perovich*, 1991]. As the incident solar radiation increases and air temperatures rise during the melt season, the ice cover evolves from a highly reflective snow-covered medium to a darker combination of bare ice, melt ponds, and leads. During the melt season there is a great degree of horizontal variability in ice surface conditions, with snow-covered ice, bare ice, ponded ice, dirty ice, and open water present. This variability in surface conditions results in a wide range of albedos, from 0.1 for leads, to 0.2–0.4 for ponds, to 0.5–0.7 for bare ice and 0.6–0.8 for snow-covered ice [*Chernigovskiy*, 1963; *Langeleben*, 1971; *Grenfell and Maykut*, 1977]. Studies of sea ice physical properties have long established that there is vertical variability in ice salinity, density,

Paper number 97JC01614.
0148-0227/98/97JC-01614$09.00

brine volume, air volume, and crystal structure [*Weeks and Ackley*, 1982]. Changes in the ice structure cause the irradiance attenuation coefficient to vary from approximately 3.5 m^{-1} at the upper surface composed of granular ice to 0.8 in the interior of the ice [*Grenfell and Maykut*, 1977]. Laboratory studies and field work have established that the albedo and transmittance for sea ice vary with wavelength. These variations are due in part to the strong spectral dependence of absorption coefficients for water, ice, and brine [*Grenfell and Perovich*, 1981; *Smith and Baker*, 1981; *Perovich and Govoni*, 1991]. Spectral signatures, particularly for transmitted light, are also influenced by the presence of biogenic material in the ice [*Maykut and Grenfell*, 1975; *Palmisano et al.*, 1987; *SooHoo et al.*, 1987; *Arrigo et al.*, 1991; *Legendre and Gosselin*, 1991].

This variability in optical properties complicates efforts to understand, and to model, radiative transfer in sea ice. Such efforts are important because of the impact that the sea ice optical properties have on problems regarding the heat and mass balance of the ice cover, and the underlying ocean water and biological activity in and beneath the ice. Since the summer melt cycle of Arctic sea ice is driven by solar radiation, understanding how the incident radiation is distributed among reflection, absorption, and transmission is important. Of particular concern is assessing the impact of the ice-albedo feedback, where small changes in climatic forcing may be amplified by the positive feedback between ice conditions and albedo. Biological activity in and under the ice is determined largely by the amount of visible light available. In contrast, ultraviolet light can be harmful and may cause decreases in both algal biomass and primary productivity [*Smith*, 1989; *Smith et al.*, 1992; *Cullen and Neale*, 1994].

The goal of this experiment was to investigate the variability of sea ice optical properties by combining optical observations with a detailed description of the physical state and structure of the ice cover. While there is considerable variation in the optical and physical properties vertically in the ice, we were also interested in putting the characteristics of this variability in the context of the spatial variability that occurs over hundreds of meters and the temporal variability that occurs over the springtime transition from cold, freezing ice to the onset of melt and the formation of melt ponds. To achieve this goal, a suite of five instruments was used to characterize the light field above, within, and below the sea ice. The optical measurements were supplemented with a characterization of the snow, the ice, and the included material. These results were combined to demonstrate the spectral, vertical, horizontal, and temporal variability of ice optical properties and to relate this variability to the physical state of the ice. This integrated effort was necessary to achieve an understanding of the processes responsible for the observed variability. The synoptic collection of this suite of measurements is the first, but vital, step toward the development and testing of integrated models linking sea ice physical and electromagnetic properties via coupled radiative transfer and ice thermodynamic-structural models.

2. Field Experiment

The field experiment was conducted in the Chukchi Sea, ~1 km offshore near Barrow, Alaska (71°N, 157°W), in 1995. The shorefast ice was predominantly first-year with several pans of multiyear ice. The field effort consisted of two segments. The first was from April 4 to April 15, when air temperatures were −15°C to −25°C and the snow cover and the ice were cold. The second was from June 5 to 15 during the onset of melt as the snow cover melted and ice surface ablation commenced.

A critical component of the experiment was obtaining a complete characterization of the physical properties of the snow and the ice. Snow depth was measured, and vertical profiles of snow stratigraphy, density, and grain size were determined; discrete snow samples were analyzed to determine particle concentrations. Surface conditions were qualitatively characterized by visual inspection and photography. Ice cores were processed to determine vertical profiles of temperature, salinity, brine volume, and density, and vertical and horizontal thin sections were made to identify the crystal structure [*Tucker et al.*, 1987]. These thin sections were also used to determine inclusion size distributions of brine pockets and air bubbles in the ice [*Perovich and Gow*, 1996]. Five-centimeter sections of the ice cores were melted and processed for the fluorometric determination of algal pigment concentrations [*Holm-Hansen et al.*, 1965], spectrophotometric determination of particulate and dissolved absorption coefficients [*Roesler and Perry*, 1995], and determination of particle type, size, and concentrations using a Galai CIS100 particle analyzer with charge-coupled device (CCD) video camera display [*Roesler and Iturriaga*, 1994].

The optical observations consisted of (1) wavelength-integrated albedo (300–3000 nm), (2) spectral albedo from the ultraviolet to the near-infrared (305–1000 nm), (3) spectral nadir reflectance in the visible and near-infrared (400–1000 nm), (4) in-ice radiance in the visible (430–680 nm), and (5) spectral transmittance in the ultraviolet and visible (305–683 nm). Albedo $\alpha(\lambda)$ as a function of wavelength λ was calculated from the ratio of the measured reflected ($E_u(\lambda)$) and incident ($E_d(\lambda)$) spectral irradiance,

$$\alpha(\lambda) = \frac{E_u(\lambda)}{E_d(\lambda)}$$

Wavelength-integrated, or total, albedo $\alpha_T(\lambda)$ was calculated from the spectral albedo integrated over the solar spectrum from 300 to 3000 nm,

$$\alpha_T = \frac{\int_{300}^{3000} E_u(\lambda)\, d\lambda}{\int_{300}^{3000} E_d(\lambda)\, d\lambda} = \frac{\int_{300}^{3000} \alpha(\lambda) E_d(\lambda)\, d\lambda}{\int_{300}^{3000} E_d(\lambda)\, d\lambda}.$$

Spectral nadir reflectance $R(\lambda)$ was determined by normalizing the reflected radiance at 0° zenith ($L_u(\lambda)$) by the reflectance from a white, diffuse Spectralon reference standard ($L_{\mathrm{ref}}(\lambda)$),

$$R(\lambda) = \frac{L_u(\lambda)}{L_{\mathrm{ref}}(\lambda)}$$

Radiance attenuation coefficients $K_L(\theta, \phi, \lambda, z)$ were calculated as the slope of a linear regression of the natural log of radiance versus depth,

$$K_L(\theta, \phi, \lambda, z) = \frac{d\{\ln [L(\theta, \phi, \lambda, z)]\}}{dz}$$

The radiance profiles were divided into 10-cm depth intervals, and the value of K_L was determined for each interval. Spectral transmittance $T(\lambda)$ is the ratio of the transmitted irradiance at

the bottom of the ice ($z = H$) to the incident irradiance on the surface ($z = 0$),

$$T(\lambda) = \frac{E_d(\lambda, H)}{E_d(\lambda, 0)}$$

Time series measurements at selected sites were used to monitor temporal changes in the measured optical properties, while transects at particular times were used to investigate spatial variability.

Five different instruments were used to make the suite of optical measurements. The total albedo was measured using a Kipp radiometer. A Spectron Engineering SE 590 spectroradiometer, with a cosine collector or a 1° field of view lens as foreoptics, was used to measure spectral albedo and reflectance at 200 wavelengths from 400 nm to 1000 nm [*Perovich*, 1991]. Ultraviolet albedo and transmittance were determined at four discrete wavelengths, 305, 320, 340, and 380 nm, using a Biospherical PUV-500 spectroradiometer. Visible transmittance was monitored at seven wavelengths centered at 413, 443, 491, 509, 555, 666, and 683 nm, with a 20-nm full-width-half-maximum band width, using a Satlantic OCP-200 spectroradiometer with cosine collector. The transmission measurements were made by mounting the visible and ultraviolet spectroradiometers on a 1-m-long "arm" with a rotating elbow joint. The arm was lowered through a 25-cm-diameter hole in the ice, so that the elbow was beneath the ice bottom. The arm of the profiler was adjusted to 90° so that the sensor of the spectroradiometer rested on the ice bottom, looking upward at 0° zenith angle. A WET Labs ice profiler was used to measure vertical profiles of in-ice radiance ($L(\theta, \phi, \lambda, z)$) at ~9-nm intervals from 430 to 680 nm. The WET Labs ice profiler consisted of a waterproof radiance detector attached to a spectroradiometer using a fiber-optic cable. A hole was drilled into the ice at a specific zenith and azimuth angle using a 10-cm-diameter core barrel. The radiance detector was attached to a pole so that the detector was oriented perpendicular to the side of the hole. Radiance profiles were obtained by lowering the detector down the hole while recording radiance and depth within the ice. By drilling holes at various angles relative to the surface of the ice and plane of the Sun, we were able to make radiance measurements at several zenith (θ) and azimuth (ϕ) angles. Radiance measurements presented in this paper are for $\theta = 90$, $\phi = 0$.

3. Results

3.1. Physical Properties of Snow and Ice

The snow cover in April was cold and did not change appreciably during the week of observations. Most of the snow cover was a wind-packed slab, consisting of 0.5-mm-diameter rounded grains, with a density of 0.36 g m^{-3}. At the base of the slab was a 2-cm-thick layer of depth hoar (10-mm-long scrolls). Snow depths were variable, with the effects of drifting evident in the surface topography. The spatial distribution of snow depth was measured every 0.5 m along a 130-m transect. The mean snow depth was 24 cm, with a standard deviation of 6 and a range from 1 to 38 cm. Particles were present in the snow, in concentrations that decreased exponentially from a maximum value of approximately 200 particles μL^{-1} at the snow-ice interface to approximately 10 particles μL^{-1} at the snow-air interface (where the microliter measurement represents a liquid volume of melted snow in order to make concentrations comparable between snows of different density). The integrated particle concentration for a 10-cm-deep snow layer was 27 particles μL^{-1}. Throughout this snow layer, the particles were predominantly spheres with diameters of approximately 1–3 μm. Within 2 cm of the snow-ice interface, larger particles with diameters of 10–30 μm were present at concentrations of 2.5–0.1 particles μL^{-1}. These larger particles were identified as aggregates of organic material.

By June the snow cover had begun to melt, and the snow density had increased to 0.41 g m^{-3}. The snow grains were 3–10 mm across and looked like smooth pebbles of ice. Water was present in the snow pack and on the surface of the ice. The state of the snow cover and the ice surface changed rapidly during this period. As the snow melted and the snow depth decreased to <0.1 m, it began to appear patchy and melting was accelerated. In only 2 days the surface changed from a uniform cover of melting snow to a variegated mixture of melting snow, superposed ice, bare ice, and ponded ice. There was a diurnal freeze-thaw cycle that may contribute to the transformation of melting snow into superposed ice. The particle concentrations for the integrated snow layers ranged from 200 to 600 particles μL^{-1}, an order of magnitude larger than the concentrations found in April. The dominant particle diameters were 2–3 μm, identified as spherical bacteria-like cells, with a significant contribution by pennate diatoms with a 5-μm-diameter minor axis. These particles were probably located in the region of the snow-ice interface, where concentrations are generally higher.

The physical properties of the ice and the included materials are summarized for April and June in Figure 1. Significant changes are evident from April to June. The ice was cold in April, with temperatures varying from −10°C to −8°C in the top 50 cm and increasing linearly with depth from 50 cm to the bottom of the ice (Figure 1a). By June the ice had warmed and was nearly isothermal, with temperatures between −2°C and 0°C. Associated with this warming was a complete desalination of the top 10 cm of the ice and a significant decrease in salinity from 10 to 50 cm (Figure 1b). As a result of ice warming, brine volumes increased, from ~3% in April to values ranging from 8% to 30% in June (Figure 1c). There was a sharp decrease in density in the upper 20 cm of the ice caused by melting and drainage from April to June. Densities below 20 cm did not change appreciably. Structurally, the ice sheet consisted primarily of columnar congelation ice, with the exception of the top 10 cm of the ice, which was granular. By a depth of 15 cm the c axes of the columnar ice crystals were oriented in the horizontal plane. At a depth of 70 cm the c axes became aligned in the horizontal plane parallel to the shore in the direction of the prevailing current [*Weeks and Gow*, 1978]. There was no appreciable change in the crystal structure of the ice from April to June, other than melt-induced retexturing of the top 10 cm.

Particle concentrations in the sea ice were generally highest at the snow-ice interface, with concentrations of approximately 100 particles μL^{-1} in both April and June, although the particle maximum extended about 20 cm downcore in June; perhaps owing to local growth of the bacterial and phytoplankton communities (Figure 1e). Concentrations of particles were also enhanced in the bottom 5–10 cm of the ice, with a concentrations factor of 5 greater found in June, again due to algal growth. The concentrations of the algal pigment chlorophyll *a* were lowest in the interior of the ice in both April and June, although the concentrations were over an order of magnitude

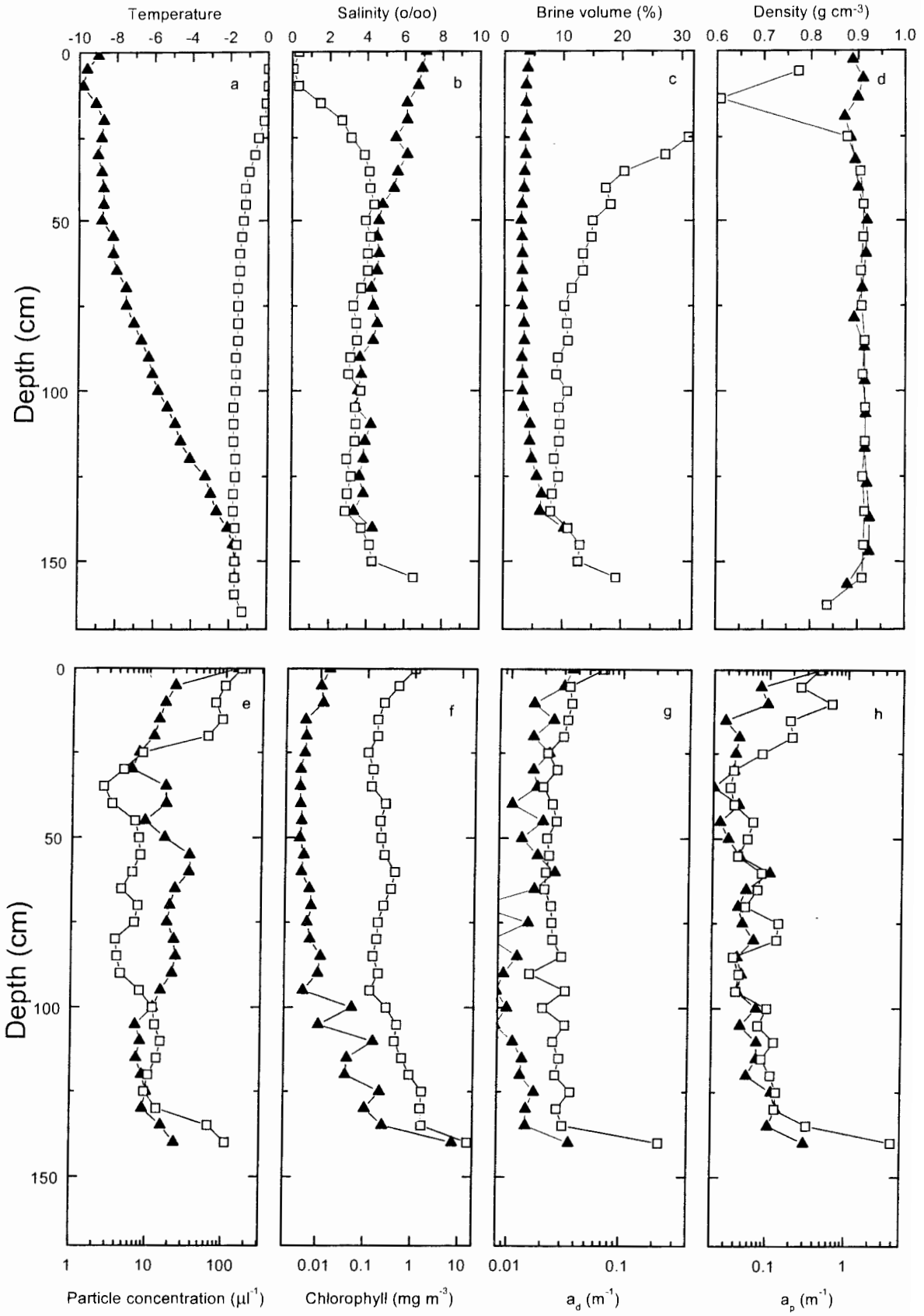

Figure 1. Vertical profiles in April (solid triangles) and June (open squares) in first-year ice of (a) temperature, (b) salinity, (c) brine volume, (d) density, (e) particulate concentration, (f) chlorophyll concentration, (g) dissolved absorption coefficient at 440 nm, and (h) particulate absorption coefficient at 440 nm.

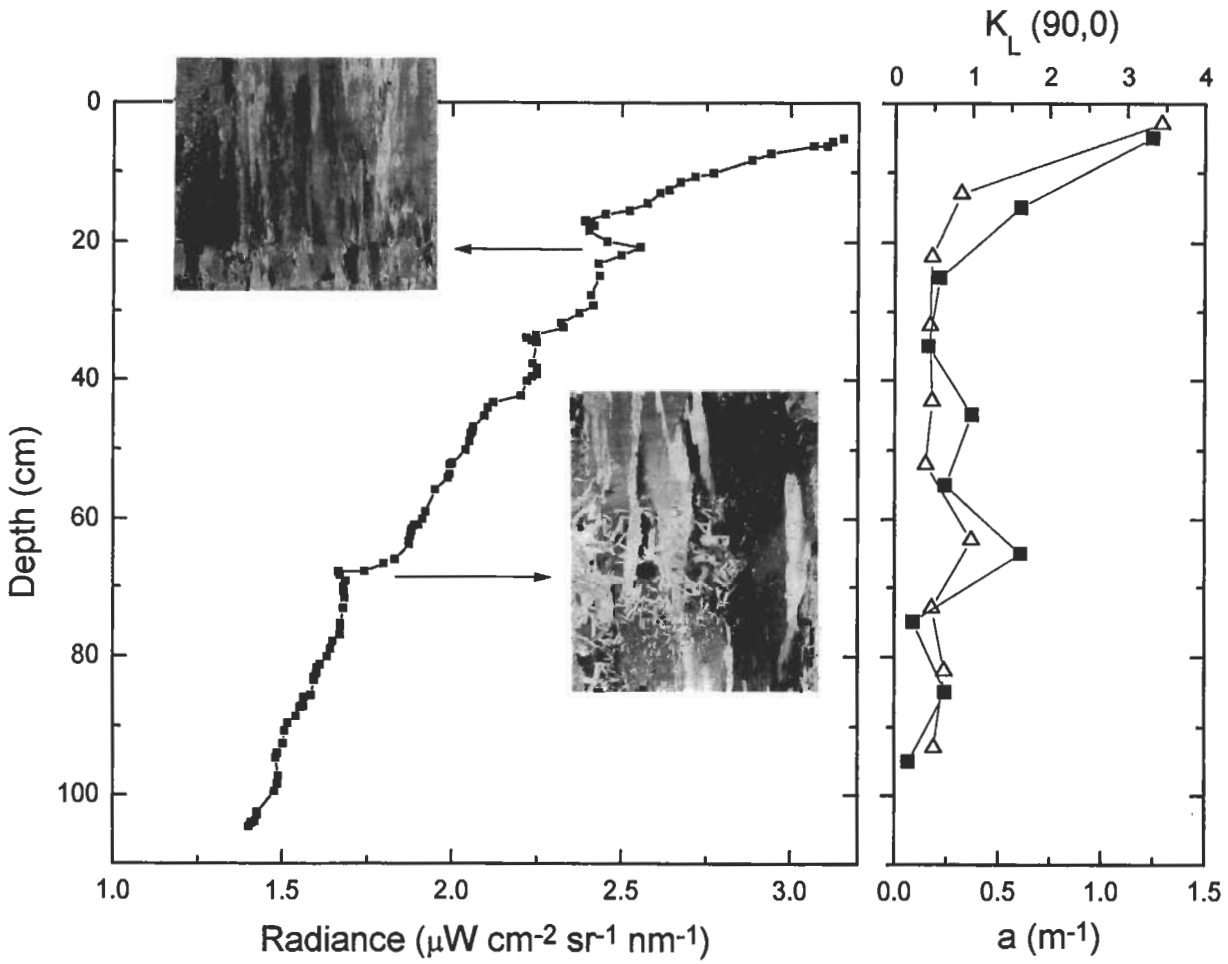

Figure 2. Vertical profiles in first-year ice in April of (left) radiance measured at 440 nm at 90° elevation, 0° azimuth and (right) associated radiance attenuation coefficient (solid squares) and measured total absorption coefficient (pure ice plus particulate plus dissolved materials) at 440 nm (open triangles). The photographic insert in the left panel are vertical thin sections viewed under polarized light for depth intervals of 16–22 cm and 55–65 cm and have a vertical scale of a few centimeters.

greater in June than in April, 0.5 versus 0.01 mg m^{-3} (Figure 1f). These concentrations are comparable to coastal and oligotrophic ocean water concentrations, respectively. The pigment concentrations were significantly greater at the ice-seawater boundary compared with the ice-snow boundary during both April and June, despite comparable interface particle concentrations. This phenomenon is likely due to increases in the algal pigment concentration per cell, a physiological response to the lower irradiance under the ice.

The absorption coefficients of the dissolved fractions of the ice samples (nominal diameter < 0.7 μm) ranged from ~0.01–0.03 m^{-1} in the interior of the ice in both April and June to 0.06–0.2 m^{-1} at the surface and bottom of the ice, respectively, in June (Figure 1g), coherent with the vertical distribution of particles and algal pigments. The absorption coefficients of the particulate fraction (nominal diameter > 0.7 μm) ranged from approximately 0.05 m^{-1} in the interior of the ice to greater than 0.2 m^{-1} in the surface and bottom samples in both April and June (Figure 1h). As with the other indicators of biotic activity, the absorption coefficients were greater in June than in April, indicating in situ accumulation of organic material.

3.2. Vertical Variability

The physical structure of the ice and the concentration of absorbing materials contained within the ice significantly impact the magnitude and spectral quality of the in-ice radiance distribution. These effects are best observed in radiance profiles and the derived attenuation coefficients. Layers of reduced or enhanced scattering can rapidly change the shape of the light field by redirecting light in a given solid angle, thus creating distinct features such as local minima and maxima in the radiance and attenuation coefficient profiles. Vertical thin sections of ice from April showed a layer with an abrupt change in the physical structure at 20-cm depth, where a visibly clear band of ice overlaid an opaque band (Figure 2). The layered structure was spatially coherent with a local minimum and maximum in the radiance profile in Figure 2. Inclusions of absorbing materials such as colored dissolved organic materials, phytoplankton, and sediments also caused variations in the vertical profiles of the radiance. A second feature was observed below 60 cm in the ice that consisted of many fine crystals embedded in the large columnar ice crystals common to the interior ice. This fine-grained layer was associated with in-

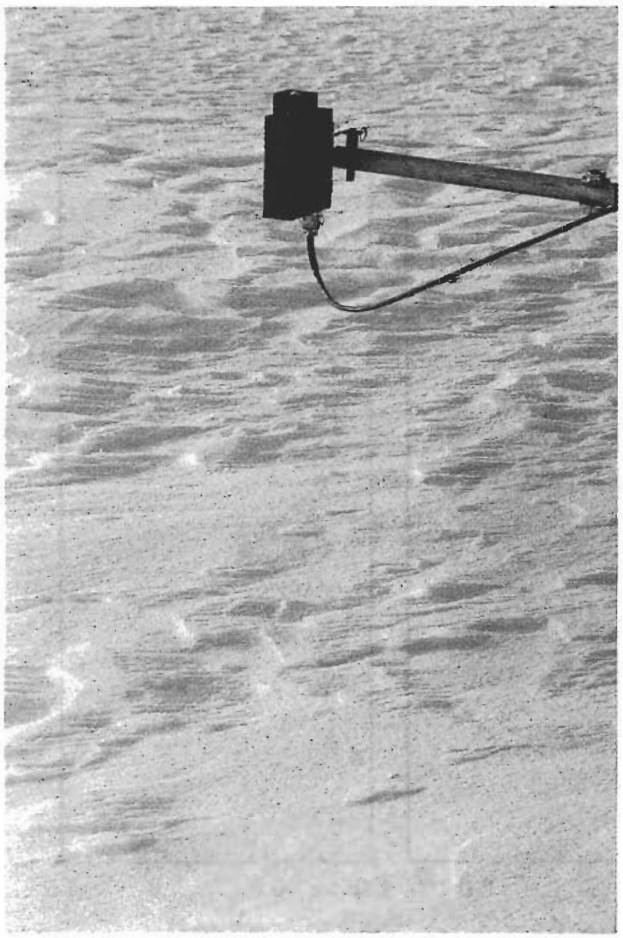

Plate 1. Snow surface topography under cold conditions in April. For scale, the instrument in the foreground is 15 cm high. The photograph was taken under sunny skies to provide maximum contrast.

creased concentrations of absorbing materials as illustrated in the right panel of Figure 2. The combination of the change in physical structure and absorbing inclusions created a sharp decrease in radiance and a local maximum in the radiance attenuation. Similarly, the upper surface layer of the ice consisted of a fine-grained ice that contains relatively high concentrations of absorbing materials, which led to the high attenuation coefficients near the surface.

Excluding the presence of these local discontinuities in the physical structure, on average the first-year ice can be described as having a surface layer 10–20 cm thick with a radiance attenuation of ~5.6 m^{-1} and interior ice with a radiance attenuation of ~0.6 m^{-1} at 440 nm. The layered structure of the ice creates considerable variability in the attenuation value of the interior ice. The standard deviation of the interior ice radiance attenuation was 0.3 m^{-1}. The relatively short-lived third layer composed of algae growing on the bottom surface of the ice in the springtime was associated with high attenuation coefficients (20–50 m^{-1}) depending upon the concentration of algae.

3.3. Horizontal Variability

To explore the horizontal variability of reflected light, we measured total albedo and spectral reflectance every 5 m along a 75-m transect in April. The footprint of the measurements was approximately 3 m^2 for the albedo and 10^{-3} m^2 for reflectance. The measurements were made on a clear, sunny day with a solar zenith angle of 67°. Ice conditions were uniform along the transect, and the thickness was 1.65 m ± 0.05 m. The ice was covered by cold, wind-packed snow with depths ranging from 0.05 m to 0.25 m. Small-scale topography was evident in the snow cover, and the surface had a rough, irregular texture. This surface roughness, and the associated bright and shadowed areas of the surface, are evident in Plate 1. Total albedos and nadir reflectances at 440 nm and 1000 nm measured along the transect are plotted in Figure 3. Snow depths at each site are presented for reference. Total albedos are large and spatially uniform, ranging from 0.73 to 0.84 with a mean of 0.78. Nadir spectral reflectance exhibited considerably more spatial variability, with values at 440 nm varying over 30% from 0.78 to 1.05. Reflectance at 1000 nm was smaller but behaved in a similar fashion. The variability of the albedo and nadir reflectance is not well correlated with the snow depth. This is not surprising, since the snow was sufficiently deep to be optically thick, so that no influence of the underlying ice was observed in the albedo. The spatial variability was due to the surface topography of the ice and the consequent irregular illumination of the surface. Minimum values were associated with areas that were shadowed somewhat, while maximum values occurred when the surface was sloped slightly toward the Sun, in a way that reflected more light (Plate 1). This explanation is consistent with the greater degree of variability shown by nadir reflectance. With a much smaller footprint than the albedo, the nadir reflectance was more sensitive to the effects of surface topography. Measurements made on cloudy, overcast days, when the direct solar beam was not distinguishable from the diffuse incident light field, showed very little spatial variability. Qualitatively, the topography of the snow surface was difficult to discern visually under these "flat light" conditions. Thus the observed variability of the ice cover was not due to any differences in the optical properties of the ice or snow but rather was due to the irregular illumination of the surface.

The spatial variability of transmitted irradiance was also measured in April along a linear transect at a nearby location in first-year ice with growth history, physical properties, and ice thickness similar to those of the albedo and reflectance transect line. The Satlantic sprectroradiometer was mounted on a submersible remotely operated vehicle and driven under the ice along a 130-m path. Snow depths were measured at 25-cm intervals along the transect. Even at the relatively transparent wavelength of 440 nm, transmittance for this cold-snow-covered ice was small, ranging from 0.2 to 0.7%. As Figure 4 indicates, there was an inverse correlation between transmittance and snow depth (correlation coefficient = 0.64), with broad trends in snow depth clearly evidenced in transmittance. However, there is not a one-to-one correspondence between small-scale fluctuations in snow depth and transmittance. Because of scattering within the snow and ice and the cosine response of the detector, a surface area of several square meters contributes to the transmitted irradiance measured at a single point, thereby smoothing the effects of small-scale irregularities in snow depth. This is evidenced by the significantly longer decorrelation length scales for transmission (3.75 m) compared with that for snow depth (2.75 m). The decorrelation length scale was defined as the lag interval when the autocorrelation coefficient was less than 0.5. A portion of the variability in the transmission that is not caused by variations in snow depth is probably due to spatial variations in the distributions of absorbing materials in the ice. While ice samples were not

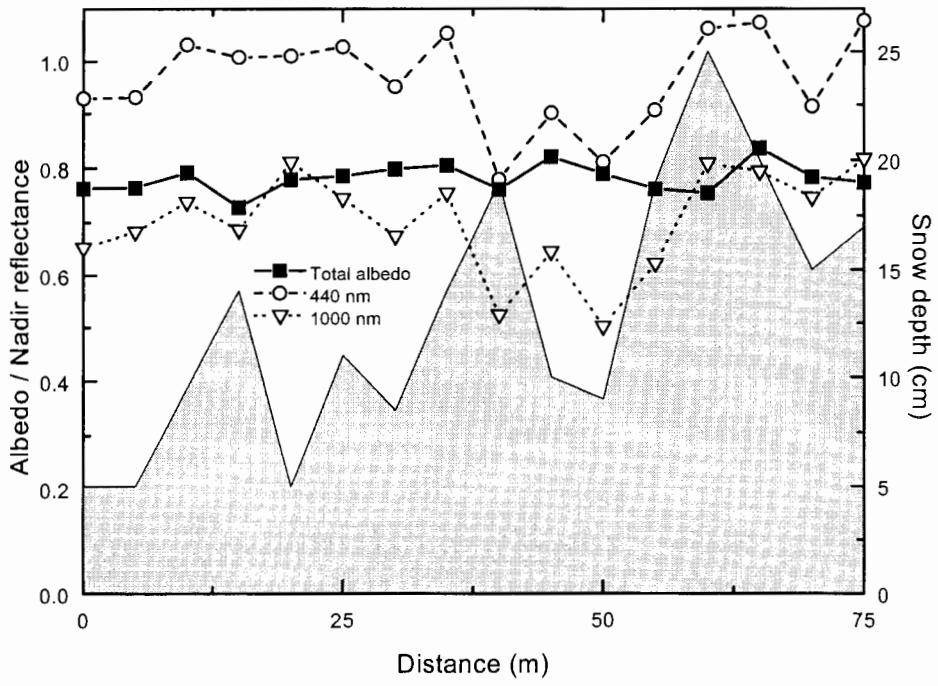

Figure 3. Horizontal transect of total albedo and nadir reflectance (400 and 1000 nm) from snow-covered ice measured in April under sunny skies with a strong solar direct beam component. The snow cover was optically thick, with depths ranging from 5 to 25 cm. The snow surface exhibited variations in topography and in texture due to drifting.

collected along this transect, the transmittance ratio of 412: 510 nm, an indicator of blue-light-absorbing organic material, varied over the transect from 0.2 to 0.7. In particular the large decrease in transmittance over the distance 110–120 m was found to correlate with a rapidly changing transmittance ratio in the absence of large changes in snow depth, suggesting that the concentrations of absorbing materials in the ice were varying in this region.

Spectral variations were also observed in the in-ice radiance spectra obtained at two sites located approximately 30 m apart in the first-year ice. At both sites the snow was shoveled from the surface of the ice to remove the influence of the snow cover. The appearance of the two ice sites was distinctly different, one appearing blue-white and the other olive green. The radiance spectrum at 20-cm depth from each of the sites indicates the effect of an enhanced concentration of absorbing inclusions in the upper surface layer of the olive green ice (Figure 5). The increase in the absorbing materials causes the

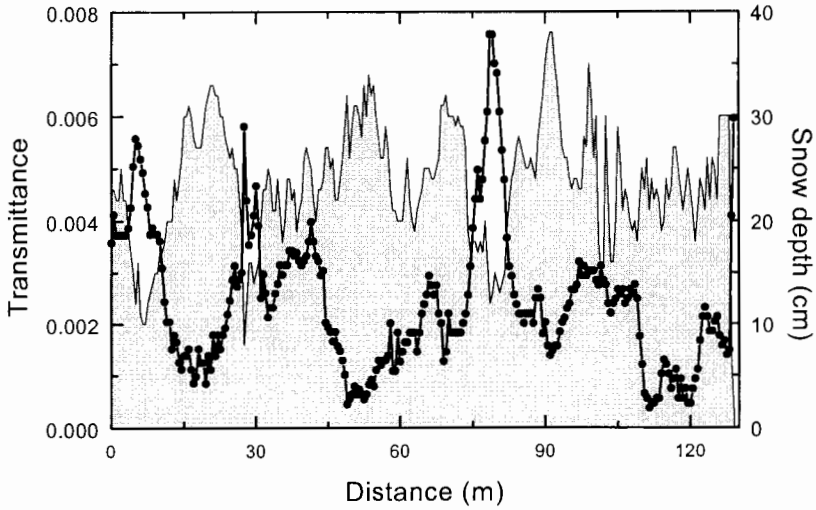

Figure 4. Horizontal transect made in April of transmittance at 440 nm (solid circles) measured within 5 cm of the ice bottom, and snow depth (shaded region).

Plate 2. Photographs of ice surface conditions on (a) April 10, (b) June 7, and (c) June 9.

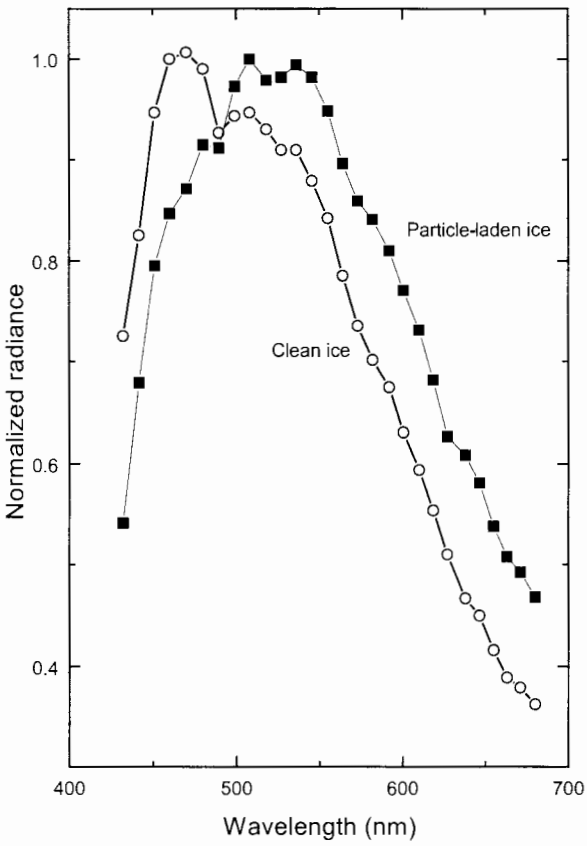

Figure 5. Normalized radiance spectra measured at a depth of 20 cm in first-year ice at two locations approximately 30 m apart. Open circles indicate clean ice, and solid squares indicate the particle-laden ice.

peak in the radiance spectrum to shift from 470 nm in the blue-white ice to 500–550 nm in the green ice. The radiance attenuation of the top 10 cm in the green ice was much higher than in the bluer ice (10.2 versus 5.6 m^{-1} at 440 nm, 9.2 versus 3.2 m^{-1} at 545 nm, and 11.6 versus 7.1 m^{-1} at 646 nm). The difference in the attenuation coefficients continued into the interior ice between 20 and 100 cm as well: 1.0 versus 0.6, 1.0 versus 0.6, and 1.7 versus 1.2 m^{-1} at 450, 545, and 646 nm, respectively. The value of the interior ice attenuation coefficient at the two sites converged below 1-m depth.

The observed layers in the radiance profiles from the two sites indicate that many of the ice features are of limited horizontal extent. The layer at 20 cm was observed at both sites, but the layer near 60 cm was not. Conversely, radiance measurements at the second olive green ice site indicate the presence of several absorbing layers that were not found in the blue-white ice shown in Figure 2.

3.4. Temporal Variability

Snow and ice conditions had changed considerably by our return in June. These changes are evident in photographs taken on April 12, June 7, and June 9, (Plate 2). By June 7 the melt season was under way, and while there was no appreciable surface or bottom ice ablation, the ice had warmed considerably and the snow cover had begun to melt. Snow depths on June 7 ranged from 0.05 m to 0.20 m. The snow cover consisted of melting "corn" snow with rounded grains several millimeters in diameter and a density of 0.40 g m^{-3}. In only 2 days, from June 7 to June 9, surface conditions changed from a uniform melting but intact snow cover to a variegated surface of melting snow, melting bare ice, and ponded ice. The ponded ice was covered by 0.05–0.10 m of meltwater.

The evolution of total albedo and the changes in spatial variability are illustrated by the three transects plotted in Figure 6. In all three cases, the measurements were made under predominant sunny skies with an unobstructed solar beam component. Total albedos for the cold-snow-covered ice on April 10 were near 0.8 and were spatially uniform with a standard deviation of 0.02. By June 7, albedos had decreased to 0.6, though the standard deviation was unchanged owing to the presence of a 0.05- to 0.10-m-thick snow cover. This decrease is a direct result of the change in the optical properties of the snow as its physical properties evolved from the cold, dry snow with submillimeter grains in April to melting, wet snow with millimeter grains in June. There was a profound change in albedo from June 7 to June 9, with an overall decrease in albedo and a large increase in the standard deviation to 0.12. Albedos ranged from 0.15 to 0.51 with a mean of 0.32 and a standard deviation of 0.12. Peak albedos were associated with areas where a few centimeters of snow cover remained, while minimum values were for 0.1-m-deep melt ponds.

A representative sequence for the spectral albedo and transmittance of first-year ice as it evolves from cold ice covered by 0.1 m of cold snow, to ice with 0.06 m of melting snow, to bare melting ice, to a 0.1-m-deep melt pond is presented in Figure 7. In all cases the ice thickness was 1.6 m, though the surface and interior conditions differed (Table 1). The bare ice studied had a thin surface layer of superposed ice, which slightly enhanced the albedo. Total albedos decreased from 0.78 to 0.60 to 0.44 to 0.20 as the ice cover warmed and melted (Table 1). As Figure 7a shows, this decrease in albedo occurs at all wavelengths. The spectral quality of the albedo also changes, with the decrease being greater in the ultraviolet and near-infrared. The spectrum changes from a flat, spectrally uniform albedo for the cold-snow-covered ice to one that is peaked in the blue (500 nm) for ponded ice.

The spectral transmittance evolved in a more complicated fashion. Naively, we would expect a corresponding increase in transmittance as the ice warmed and the albedo decreased. This was not the case. Transmittance for the melting-snow-covered ice was less at all wavelengths than for the cold-snow-covered ice. This was a direct result of light absorption by algae in the skeletal layer at the bottom of the ice. The algal biomass increased from approximately 0.75 to 15.43 mg Chl m^{-3}, an increase that was visibly evident in the ice cores as a brown layer on the bottom. The spectral shape of the transmittance for the melting snow case is consistent with light absorption in an algal layer [*Maykut and Grenfell*, 1975; *Arrigo et al.*, 1991; *Fritsen et al.*, 1992; *Zeebe et al.*, 1996], with enhanced attenuation in the ultraviolet and the maximum transmission shifted to longer wavelengths (555 nm). As is indicated by comparing the transmittance at 320 nm and the transmitted PAR (Table 1), attenuation by the algae and their associated particulate and dissolved organic material was larger in the ultraviolet than in the visible. The transition from melting snow to bare ice substantially decreased the albedo and tended to increase the transmittance. However, there were still significant amounts of algae present in the ice (1.62 mg Chl m^{-3}), which strongly reduced ultraviolet transmittance and to a lesser extent blue light levels. The transmittance results from the cold snow and melting snow cases demonstrate the significant impact that

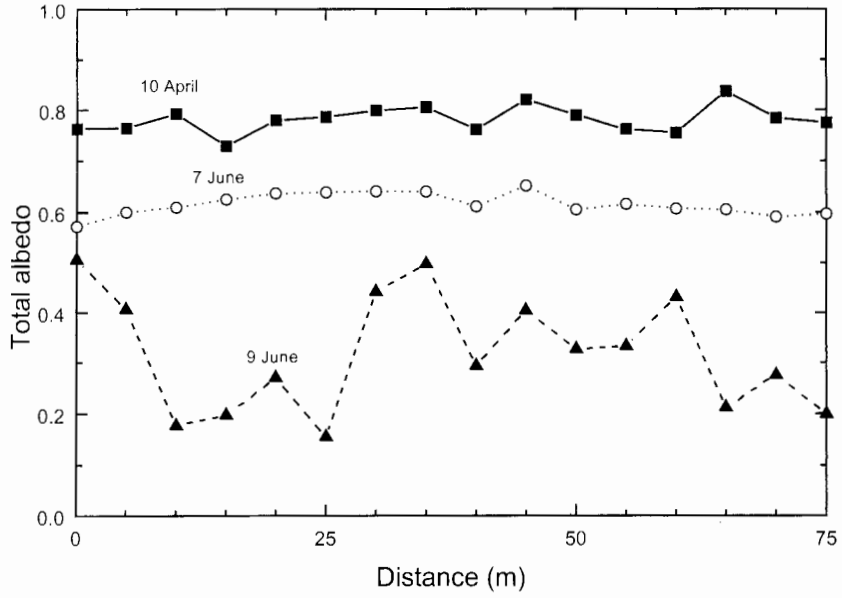

Figure 6. Total albedo measured every 5 m along a 75-m transect on April 10, June 7, and June 9. All three sets of measurements were made under sunny skies with a strong solar direct beam component.

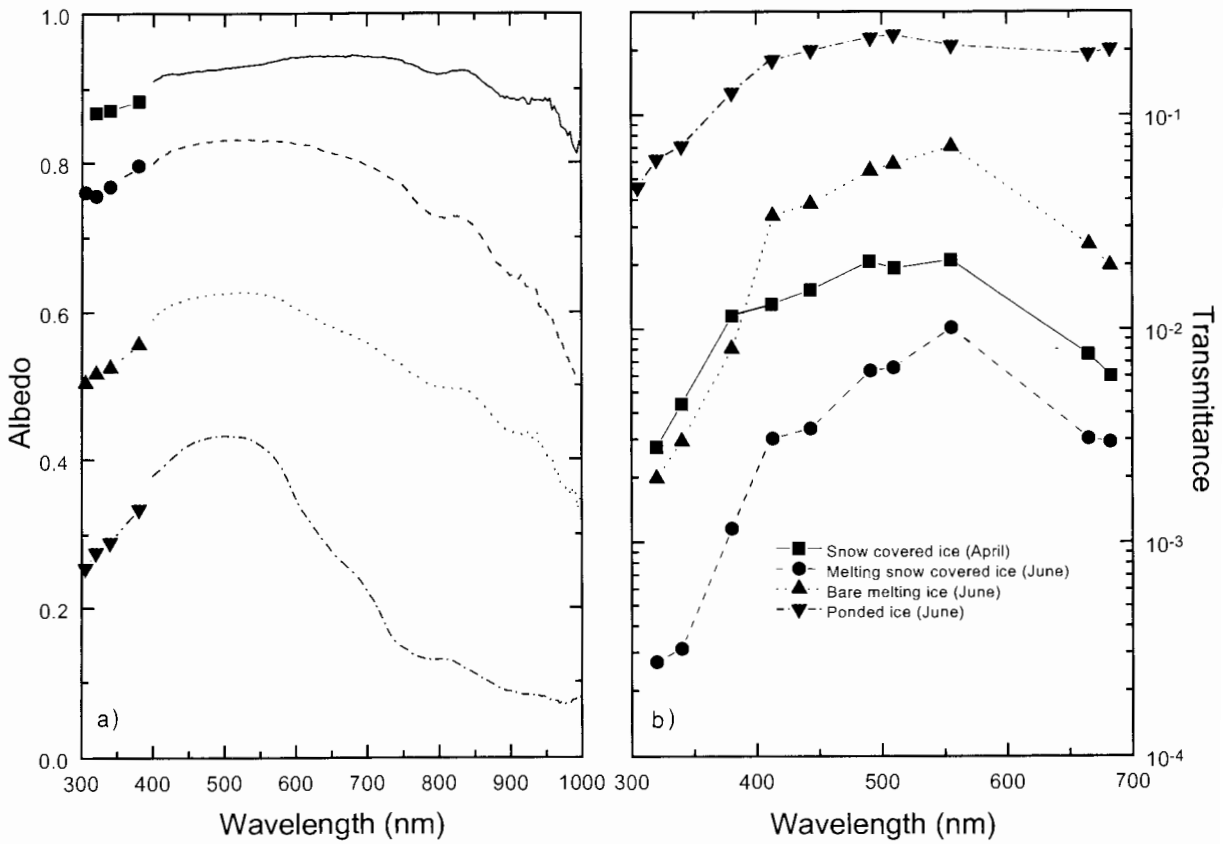

Figure 7. The evolution of (a) spectral albedo and (b) spectral transmittance during the onset of melt. Results are presented for 0.1 m of cold snow over ice, 0.06 m of melting snow over ice, bare melting ice and a 0.1-m-deep melt pond The ice thickness was approximately 1.6 m in all cases. There were significant concentrations of algae present in the skeletal layer at the bottom of the ice for both the melting snow-covered ice and the bare ice cases.

Table 1. Summary of Optical Evolution of First-Year Ice

	Date	Sky	θ, deg	H_s, cm	H_i, cm	Chl, mg m^{-3}	Albedo			Transmitted			Absorbed		
							320 nm	PAR	Total	320 nm	PAR	Total	320 nm	PAR	Total
Cold-snow-covered ice	April 7	SDCV	15	10	164	0.75	0.870	0.897	0.780	0.003	0.018	0.009	0.127	0.086	0.211
Melting-snow-covered ice	June 8	BC	29	6	162	15.43	0.760	0.803	0.600	0.000	0.005	0.004	0.240	0.192	0.396
Bare melting ice	June 8	BC	43	0	162	1.62	0.520	0.581	0.440	0.002	0.021	0.029	0.478	0.398	0.531
Ponded ice	June 9	BC	41	6*	160	n.a.	0.290	0.347	0.200	0.062	0.144	0.128	0.648	0.509	0.672

Sky conditions are SDCV (hazy, solar disk clearly visible) and BC (bright, clear skies). H_s is the snow depth except as noted, H_i is the ice thickness, and Chl is the chlorophyll *a* concentration in the bottom 5 cm of the ice column. PAR refers to photosynthetically active radiation integrated from 400 to 700 nm, and total is integrated from 400 to 2400 nm.

*Melt pond depth H_p.

biogenic material can have on light transmission through sea ice. Finally, for the ponded ice case, scattering and attenuation in the ice were much less than in the other cases and the bottom algae were gone, resulting in the highest observed transmittance. In this case, 13% of the total incident solar irradiance, 20% of the visible, and 5–15% of the ultraviolet was transmitted, demonstrating that significant amounts of solar energy can be transmitted to the ocean through melt ponds.

Shorter-timescale variations in spectral albedo and transmission were observed with twice-daily measurements over a period of $2\frac{1}{2}$ days. From morning to evening on June 8 the thin layer of snow melted, and the surface of the ice began to pond. The albedo at 440 nm decreased from 0.63 to 0.37. The increasing concentration of algae in the skeletal layer caused the transmission to decrease slightly from 0.034 to 0.029. By late morning of June 9 the algal layer, in response to increased light transmission at the surface of the ice due to ponding, dropped off the skeletal layer at the bottom of the ice (a phenomenon that has been observed previously [*Cota and Horne*, 1989; *Perovich et al.*, 1993]) resulting in an increase in transmission beneath the ice to approximately 0.042. The albedo did not change appreciably. From the evening of June 9 to the late morning of June 10 we observed drainage of the ponded water, increased porosity of the ice surface, increased albedo to 0.53, and decreased transmittance to 0.023.

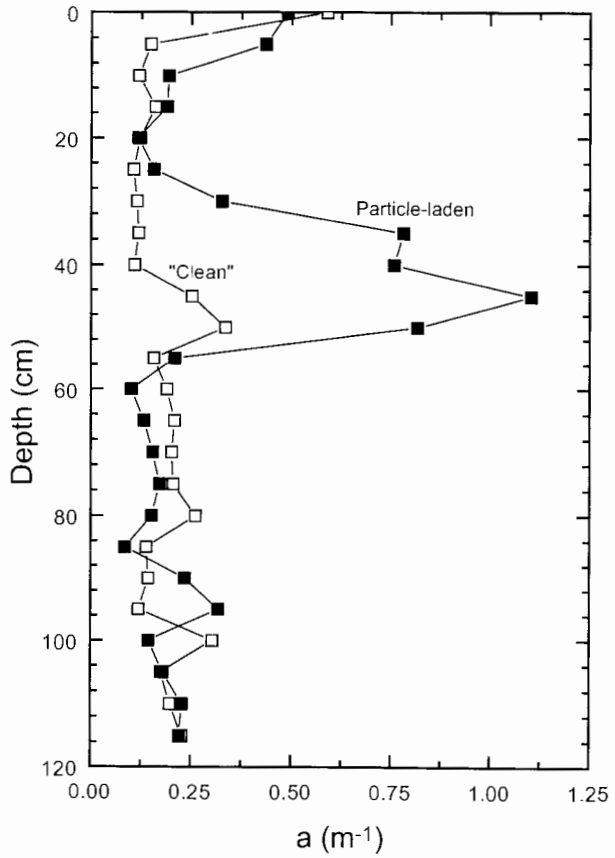

Figure 8. Vertical profiles of total (pure ice plus particulate plus dissolved materials) absorption coefficients at 440 nm for the "clean" hummock and particle-laden refrozen melt pond on the multiyear ice floe in April.

Radiance measurements were conducted at the same location as were the June albedo and transmission measurements, approximately 40 m from the April sites. The measurements were not made within a melt pond. Drainage of nearby melt ponds did, however, occur when holes were drilled. There was no significant difference in the radiance attenuation coefficients for the interior ice (40- to 150-cm depth) measured at the June site and those of the April sites. The low-density surface layer (Figure 1d) in June did cause modification to the radiance attenuation profile. As the light passed from the low-density surface ice to the interior ice, negative radiance attenuation values were observed. The negative radiance attenuation values are an indication of a rapid change in the shape of the radiance distribution when the light passes from the surface to interior ice. The attenuation at the bottom surface of the ice may have also changed owing to the increased biological material contained at this interface. We did not, however, make radiance measurements through the bottom layer in April; therefore we cannot confirm this change using radiance measurements.

3.5. Multiyear Ice

3.5.1. April. While our primary focus was on the optical properties of first-year ice, there was an opportunity to investigate a floe of multiyear ice that was entrapped in the first-year ice. This multiyear pan contained several hummocks and melt ponds. Measurements were made in April in a frozen melt pond from the previous summer and a hummock separated by less than 3 m. Ice from the frozen melt pond contained large quantities of particulate inclusions, while ice from the hummock had much lower concentrations. The absorption coefficients (particulate plus dissolved) at 440 nm for the surface layer at both multiyear ice sites were approximately 0.5 m^{-1}, comparable to those for the first-year ice (Figure 8). The absorption coefficients for the interior multiyear ice were about a factor of 2 larger than for the first-year ice. The base of the frozen melt pond at approximately 45 cm had very large absorption coefficients of greater than 1.0 m^{-1}. While there is a

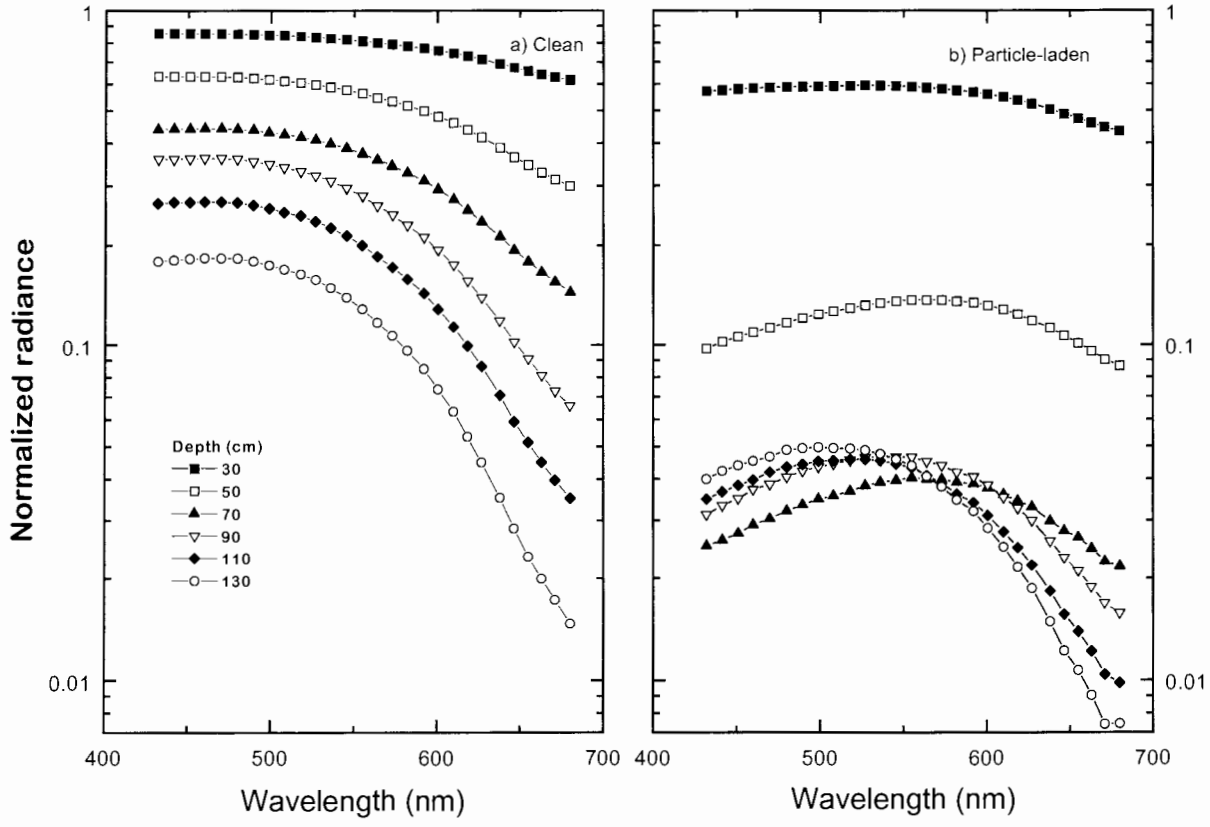

Figure 9. April measurements of spectral radiance normalized to values at 10 cm for discrete depths in the multiyear ice floe for (a) the "clean" hummock and (b) the particle-laden refrozen melt pond.

slight absorption maximum at a depth of 50 cm in the clean hummock ice, we feel this is coincidental, as the structure of the ice at the two sites was very different.

Spectral radiance was measured in the particle-laden melt pond region and in the "clean" hummock. Results normalized to values measured at 10 cm are plotted in Figure 9. The radiance attenuation at 440 nm was 0.8 m^{-1} in the hummock, with attenuation that slowly increased with increasing wavelength due to the greater absorption by ice at the longer wavelengths. The radiance therefore was primarily at blue wavelengths at depths of a meter or greater. This was observed visibly as very deep blue light emanating from the core hole. The radiance within the frozen melt pond was much more complicated; light emanating from the core hole appeared dark olive green. The large particle load in the ice created a high attenuation in the upper 70 cm (2–10 m^{-1} at 440 nm). The inclusions in the ice absorb predominantly in the blue region, causing the peak in the spectral radiance to shift to 550 nm as can be seen at the 50- and 70-cm levels. The limited horizontal extent of the melt pond feature allowed light to be scattered in from the surrounding "clean" ice at depths greater than 70 cm. This effect is most dramatic in the blue wavelength region, where light scattered from the surrounding "clean" ice caused an increase with depth in the blue portion of the radiance below the melt pond. The increase in blue light also shifts the spectral quality of the light beneath the "dirty" pond toward the "clean" hummock ice case.

Spectral albedos for the multiyear hummock and refrozen melt pond were measured upon removal of approximately 10 cm of snow (Figure 10). The clean ice was characterized by a peak in albedo of approximately 0.74 at 490 nm. The particle-laden melt pond exhibited a peak in albedo of 0.66 at 550 nm, with a strong decrease in albedo towards the blue end of the spectrum due to the strong absorption by the entrapped particulate material. Not surprisingly, the spectral shapes of the albedos for these two cases were very similar to the spectral shapes of the radiance distributions measured at approximately 70 cm, indicating that for snow-free ice, materials entrapped at such depths do influence the spectral quality and quantity of reflected irradiance.

3.5.2. June. Spectral albedos for a multiyear hummock and three multiyear melt ponds were measured in June on the same multiyear pan as in April (Figure 11). Both the hummock and the refrozen melt pond from April were found to be melt ponds by June (comparable to the white pond and dirty pond in Figure 11). The spectral albedo for the multiyear hummock was larger than any of the other bare ice cases and was comparable to that for the melting snow. The spectral albedo was fairly constant across the visible part of the spectrum, and indeed the hummock looked white. Visible inspection of an ice core from the top portion of the hummock confirmed that it contained many more air bubbles, and consequently more scattering, than the first-year ice. Adjacent to the hummock was a low area where the bubbly white ice was covered by approximately 15 cm of meltwater. This melt pond appeared white, since the underlying ice was bubbly like that of the hummock. The presence of the water in this white melt pond caused a decrease in total albedo from 0.61 to 0.37. The reduction was greatest at longer wavelengths, with the near-infrared albedo decreasing to less than 0.2, while in the visible the decrease was only from approximately 0.77 to 0.65, with the melt pond retaining a whitish appearance. This spectral behavior is well

established and is a result of the increasing opacity of water in the infrared [*Grenfell and Maykut*, 1977; *Grenfell and Perovich*, 1984]. At these wavelengths, absorption in the water is so large that albedo is determined by surface reflection. In the visible, however, the spectral albedo is governed by the properties of the underlying ice and the depth of the pond. As these parameters vary, so does the pond albedo. Spectral albedo measurements for the white, blue, and dirty ponds illustrate this point. The underlying ice in the blue pond had notably fewer bubbles than the ice in the white pond, and visible albedo was roughly 20% smaller than that for the white ice. The dirty pond is a more extreme case where the pond was much deeper, approximately 0.7 m, and the bottom was visibly dirty, with large quantities of particulates. The depth of the pond caused a significant reduction of the albedo at visible wavelengths. The presence of the particulates further decreased the magnitude of the albedo and caused a distinctive peak at 550 nm in the spectrum.

4. Discussion

The physical structure of sea ice is important in determining the structure of the associated light field. The addition of absorbing materials within the ice causes a reduction in the radiance at all angles. Changes in the scattering properties, both in magnitude and in angular distribution, may be related to gradients in the physical structure of the ice as well as the included particulate materials. Changes in the angular distribution of the scattering cause variations in the shape of the radiance distribution, increasing the radiance at some angles while decreasing it at others. The scattering within the ice also tends to act as a low-pass filter, smoothing out features that have small horizontal extent as seen in the horizontal transects of transmittance and in the light field under the frozen melt pond on the multiyear ice.

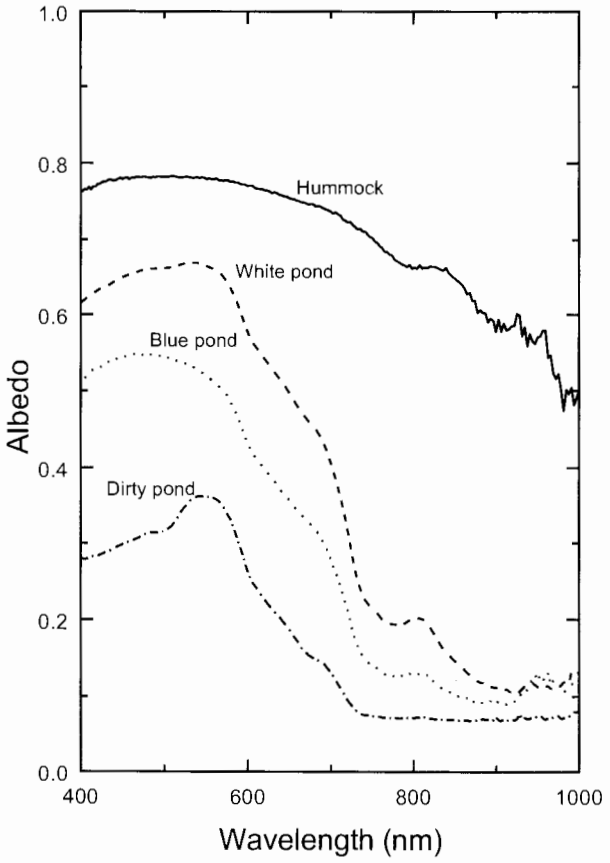

Figure 11. June measurements of spectral albedos for a hummock and three melt ponds in the multiyear ice floe. The observations were made under a complete cloud cover with the solar disk barely visible. The cases were a multiyear hummock (α_T = 0.61), a white pond with bubbly ice under 15 cm of meltwater (α_T = 0.37), a 15-cm-deep blue pond (α_T = 0.29), and a 70-cm-deep dirty pond (α_T = 0.17).

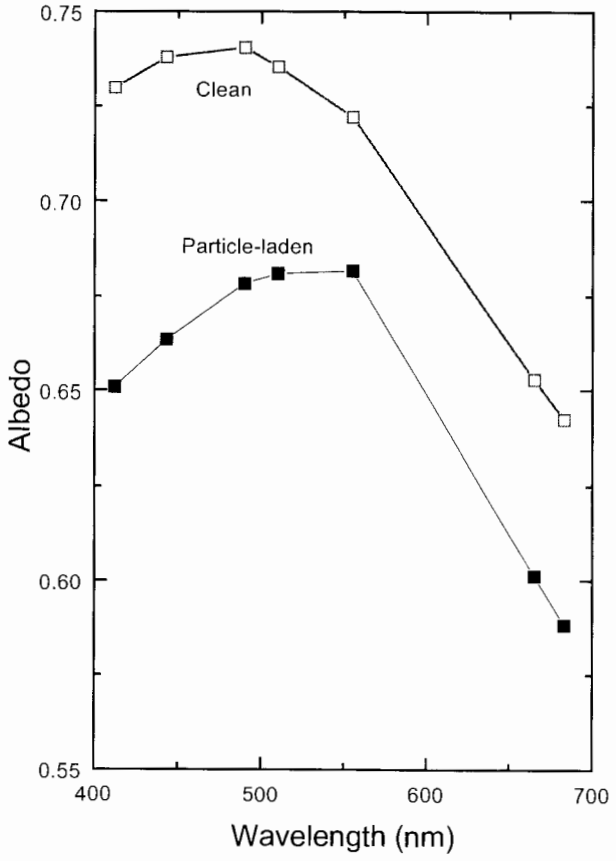

Figure 10. April measurements of spectral albedos for the "clean" hummock and particle-laden refrozen melt pond in the multiyear ice floe. The snow was removed from both sites to observe solely the signal from the ice and entrapped materials.

Layers within the ice that affect the radiance distribution can have three sources: those related to changes in physical structure, those related to changes in absorbing inclusions, and those in which both of the previous mechanisms are present. Changes in the physical structure may be related to changes in the formation mechanism (e.g., frazil to congelation transitions), the growth conditions (e.g., crystal orientation, alignment, bubble density, or growth rate), and metamorphic processes (melting, brine drainage). The springtime biological layer on the underside of the ice is a good example of the influence of absorbing materials, although this phenomenon is relatively short-lived compared with the less dramatic but temporally persistent in-ice distributions of absorbing material. In many cases the physical structure and enhanced concentrations of inclusions are spatially coherent. Frazil ice formation in the fall is the foundation of the surface sea ice layer of the ice that we studied. Frazil ice incorporates phytoplankton, dissolved organics, or resuspended sediments contained within the sea-

water [*Garrison et al.*, 1983, 1990; *Pfirman et al.*, 1990; *Reimnitz et al.*, 1990; *Ackley and Sullivan*, 1994]. The surface ice layer therefore has a fine-grained structure and enhanced concentrations of incorporated materials. It is important to note that for both seasons, particle concentrations were high at the snow-ice interface. Algal cells transported by brine wicking in the spring are left behind after drainage occurs. These particles undergo growth, increasing in concentration and resulting in increased absorption of shortwave radiation at the interface during the melting season.

The slower growth of large-grained congelation ice beneath this fine-grained layer has a very different physical structure that is not as conducive to particle entrapment. The mechanism associated with the structure and particle loading seen around 60 cm in Figure 2 is more difficult to explain. It is possible that the particles were trapped during the normal ice growth and the change in physical structure is related to metamorphism of the ice by localized heating because of the higher absorption by the particles [*Fritsen et al.*, 1992; *Zeebe et al.*, 1996]. The small crystals observed may also be related to a freezing mechanism such as a sub-ice frazil layer [*Dieckmann et al.*, 1986] or buoyant anchor ice [*Reimnitz et al.*, 1987] that brought the particles to the ice surface. Regardless of the mechanism, the relationship between ice structure and absorbing inclusions is important for improving our understanding of the light field associated with sea ice.

Qualitatively, the temporal changes in ice optical properties during the onset of melt are straightforward to understand. A reduction in scattering causes a decrease in albedo and an increase in transmittance. Melting induces physical changes in the snow and ice that tend to reduce scattering within the medium. As melting occurs in the snow cover, the grain size increases and a portion of the air void fills with meltwater, both of which decrease scattering. The presence of meltwater on the ice surface reduces scattering and consequently the albedo, particularly at longer wavelengths [*Grenfell and Maykut*, 1977]. Warming in the interior of the ice increases the brine volume and, at least initially, reduces large angle scattering as brine pockets grow and interconnect, increasing the size and reducing the number of scatterers [*Perovich and Grenfell*, 1981]. During pond development in the first-year ice, there was a continual and considerable percolation of air bubbles to the surface of the ponds. We believe that the source of this percolation was the release of air bubbles from the interior of the melting ice. The melting-induced reduction in scattering can be mitigated if the ice drains. In this case, water-filled voids become air-filled voids, and scattering within the ice increases. For example, the upper 0.5 m of the multiyear hummock was above freeboard and contained numerous air bubbles, and it had an albedo that was larger than that of any of the other bare ice cases and comparable to that of melting snow.

The partitioning of the solar radiation incident on an ice cover between reflection to the atmosphere, absorption in the ice, and transmission to the ocean has a significant impact on the heat and mass balance of the ice cover. This partitioning is governed by the optical properties of the ice and exhibits both spatial and temporal variability. In fact, the seasonal progression of reflection, absorption and transmission are not temporally coherent as might be expected. The temporal variability in light partitioning is explored in Table 1, where a time series of the light reflected by, absorbed in, and transmitted through the ice is presented. Albedo tends to decrease as the melt progresses. Consider, for example, the changes attendant with the decrease in albedo between June 7 and June 9. The incident solar irradiance was large during this period, averaging 300 W m^{-2}. The solar energy that is not reflected contributes primarily to surface or internal melting of the ice, with a small fraction transmitted to the underlying water. The albedo, averaged over the transect, decreased from 0.62 to 0.32. This resulted in an additional 90 W m^{-2} of heat input to the ice cover, which is equivalent to approximately 0.03 m of ice melt per day. A similar trend in albedo and absorption is evident in the first-year ice evolutionary sequence presented in Figure 7 and summarized in Table 1. As melting progressed there was a steady decrease in albedo and increase in the amount of energy absorbed in the ice cover. For the April cold-snow-covered case, only 21% of the incident radiation is absorbed, virtually all of it in the snow. During the melt season in June the absorption increases to 40% for the melting-snow-covered case, to 53% for the bare ice and 67% for the melt pond. This reduction in albedo and increase in absorption leads to additional melting, which in turn tends to lower the albedo. This is the ice-albedo feedback mechanism.

Melt ponds are believed to play a critical role in the ice-albedo feedback and in the summer melt cycle of sea ice. The presence of melt ponds reduces the albedo, enhances surface ablation, and increases optical transmission to the ocean. Because of this potential importance, recent large-scale sea ice thermodynamic models include melt ponds [*Ebert and Curry*, 1993; *Ebert et al.*, 1995]. During the height of the melt season, ponds can cover a substantial fraction of the ice. For example, Plate 3 is an aerial photograph of a 500- by 700-m area of the Beaufort Sea (76°N, 172°W) on July 30, 1994. A survey of a 20-km^2 area showed that the ice concentration was 94% and that ponds covered 13% of the ice area. For simplicity, models typically assume that all ponds have similar optical properties. However, our results illustrate that there is a wide range of melt pond spectral and total albedos and indicate that this variety results from differences in pond depth and the properties of the underlying ice, including variations in the particle concentrations in the surface frazil ice layer.

A close examination of Plate 3 shows that while ponds are easily distinguishable from leads and bare ice, they also exhibit differences among themselves, with dark blue, blue, light blue, green, and whitish ponds present. Not only are these ponds different colors, but the magnitude of their total albedo can differ by as much as a factor of 2. There have been several studies of melt pond albedos [*Langleben*, 1969, 1971; *Grenfell and Maykut*, 1977; *Grenfell and Perovich*, 1984], but little is known regarding the optical properties of the pond ice or transmission through the ponds. Information is also scarce regarding the physical properties of ponded ice. *Tucker et al.* [1987] reported on the salinity, density, and crystal structure of ponded ice, and *Shokr and Sinha* [1994] reported air bubble size distributions for a first-year melt pond. To assess the impact of melt ponds on sea ice thermodynamics, additional information is needed concerning the areal extent, the temporal duration, and the water content of melt ponds. Plate 3 illustrates that pond coverage can be obtained from aerial photography, and areally averaged albedos can be measured using aircraft-mounted radiometers [*Langleben*, 1971]. It may be possible to use spectroradiometers to exploit the spectral differences in pond albedo to estimate pond depth and the properties of the underlying ice. Qualitatively, we know that bluer ponds tend to be deeper, green ponds denote the presence of algae and other organic material, and white ponds are

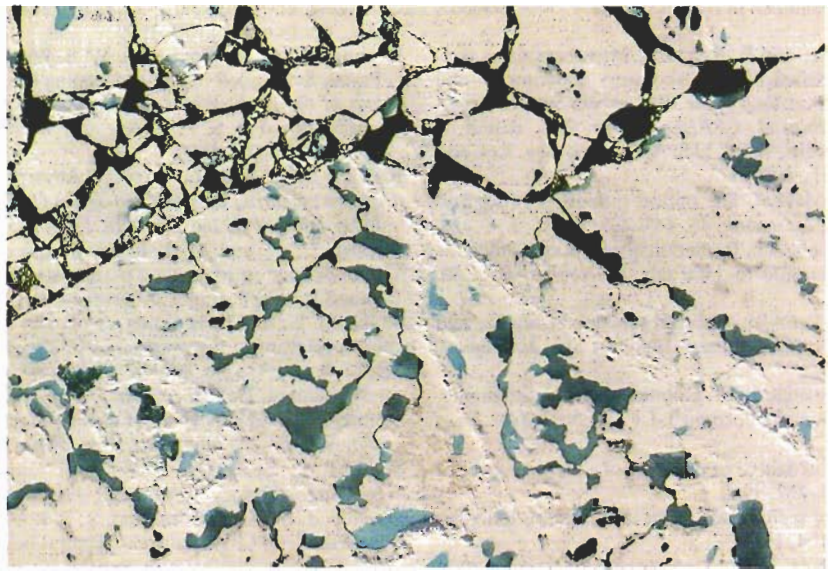

Plate 3. Aerial photograph of sea ice during the height of the melt season, taken at 76°N, 172°W on July 30, 1994. Photograph courtesy of W. B. Tucker III.

shallow with bubbly ice below. By combining additional field studies and with a comprehensive radiative transfer model for melt ponds, it may be possible to estimate pond depth and ice properties quantitatively from observations of spectral albedo.

5. Conclusions

During the annual spring-to-summer transition, there is a general decrease in albedo and a concomitant increase in absorbed and transmitted light. Changes in albedo are dominated by changes in surface conditions. As the snow melts and the ice surface becomes a variegated mixture of melting snow, bare ice, and ponded ice, the average albedo decreases and the horizontal variability in albedo increases. While absorption and transmission are affected by the surface conditions, they are also dependent on interior properties and algal blooms on the underside of the ice. The solar radiation absorbed in the ice exhibits a seasonal progression, with maximal values during the bloom of algae on the underside of the ice and during the melt pond period, when more radiant energy enters the ice cover. Visible wavelength albedo for melt ponds is influenced not only by the pond depth but also by the properties of the underlying ice.

The radiance distribution within the ice is strongly affected by the particulate and dissolved materials contained within the ice. While the distribution of inclusions causes variations in the attenuation, the typical value for the interior of first-year ice over the spectral range of 430–550 nm is 0.8 m^{-1}. At longer wavelengths the attenuation increases as absorption by the ice becomes more important.

This extensive data set provides an excellent resource for the development and evaluation of optical models of sea ice and its constituent components. Such models are necessary to fully understand and represent the temporal and spatial variability of optical properties. Future efforts need to be directed toward incorporating these observational results into radiative transfer models and toward extending the small-scale measurements of the optical properties of individual ice types to estimate the large-scale optical properties of the ice cover.

Acknowledgments. This work has benefited greatly from the contributions of several individuals. We would like to thank Elizabeth Bruce of WET Labs for her help in developing and deploying the Ice Profiler, Jesse Collins of the Polar Ice Coring Office for developing and operating the ice coring devices, Bruce Elder and Rebecca Hansing for their able assistance in making the field measurements, Robert Maffione and Curt Mobley of SRI International for helpful discussions regarding the development and deployment of the Ice Profiler and for use of their ice coring rig, Nancy Perron for thin section preparation, Jennifer Simeon for ice sample analyses, and Jeff Voss of SRI International for his assistance in making the radiance measurements. Lewis Shapiro and William Zito of the University of Alaska, Fairbanks, are gratefully acknowledged for providing and operating the Mitsui ROV for the transects of under-ice transmittance. This work was funded by the Office of Naval Research, Ocean Optics Program, as part of an accelerated research initiative on the electromagnetic properties of sea ice, under contracts N00014-93-10149, N00014-95-10720, N00014-93-10124, and N00014-95MP-30002.

References

Ackley, S. F., and C. W. Sullivan, Physical controls on the development and characteristics of Antarctic sea ice biological communities: Review and synthesis, *Deep Sea Res.*, *41*, 1583–1604, 1994.

Arrigo, K. R., C. W. Sullivan, and J. N. Kremer, A bio-optical model of Antarctic sea ice, *J. Geophys. Res.*, *96*, 10,581–10,592, 1991.

Chernigovskiy, N. T., Radiational properties of the central Arctic ice cover (in Russian), *Tr. Arkt. Antarkt. Nauchno Issled. Inst.*, *253*, 249–260, 1963.

Cota, G. F., and E. P. W. Horne, Physical control of ice algal production in the high Arctic, *Mar. Ecol. Prog. Ser.*, *52*, 111–121, 1989.

Cullen, J. J., and P. J. Neale, Ultraviolet radiation, ozone depletion, and marine photosynthesis, *Photosynthesis Res.*, *39*, 303–320, 1994.

Dieckmann, G., G. Rohardt, H. Hellmer, and J. Kipfstuhl, The occurrence of ice platelets at 250 m depth near the Filchner Ice Shelf and its significance for sea ice biology, *Deep Sea Res.*, *33*, 141–148, 1986.

Ebert, E. E., and J. A. Curry, An intermediate one-dimensional thermodynamic sea ice model for investigating ice-atmosphere interactions, *J. Geophys. Res.*, *98*, 10,085–10,109, 1993.

Ebert, E. E., J. L. Schramm, and J. A. Curry, Disposition of solar radiation in sea ice and the upper ocean, *J. Geophys. Res.*, *100*, 15,965–15,975, 1995.

Fritsen, C. H., R. Iturriaga, and C. W. Sullivan, Influence of particulate matter on spectral irradiance fields and energy transfer in the eastern Arctic Ocean, in *Ocean Optics 11*, *Proc. SPIE Int. Soc. Opt. Eng.*, *1750*, 527–541, 1992.

Garrison, D. L., S. F. Ackley, and K. R. Buck, A physical mechanism

for establishing algal populations in frazil ice, *Nature*, *306*, 363–365, 1983.

Garrison, D. L., A. R. Close, and E. Reimnitz, Microorganisms concentrated by frazil ice, evidence from laboratory experiments and field measurements, in *Proceedings of the W. F. Weeks Symposium on Sea Ice Properties and Processes*, *CRREL Monogr. 90-1*, edited by S. F. Ackley and W. F. Weeks, 92–96, U.S. Army Cold Reg. Res. and Eng. Lab., Hanover, N. H., 1990.

Grenfell, T. C., and G. A. Maykut, The optical properties of ice and snow in the Arctic Basin, *J. Glaciol.*, *18*, 445–463, 1977.

Grenfell, T. C., and D. K. Perovich, Radiation absorption coefficients of polycrystalline ice from 400 to 1400 nm, *J. Geophys. Res.*, *86*, 7447–7450, 1981.

Grenfell, T. C., and D. K. Perovich, Spectral albedos of sea ice and incident solar irradiance in the southern Beaufort Sea, *J. Geophys. Res.*, *89*, 3573–3580, 1984.

Holm-Hansen, O., C. J. Lorenzen, R. W. Holmes, and J. D. Strickland, Fluorometric determination of chlorophyll, *J. Cons. Int. Explor. Mer.*, *30*, 3–15, 1965.

Langleben, M. P., Albedo and degree of puddling of a melting cover of sea ice, *J. Glaciol.*, *8*, 407–412, 1969.

Langleben, M. P., Albedo of melting sea ice in the southern Beaufort Sea, *J. Glaciol.*, *10*, 101–104, 1971.

Legendre, L., and M. Gosselin, In situ spectroradiometric estimation of microalgal biomass in first-year sea ice, *Polar Biol.*, *11*, 113–115, 1991.

Maykut, G. A., and T. C. Grenfell, The spectral distribution of light beneath first-year sea ice in the Arctic Ocean, *Limnol. Oceanogr.*, *20*, 554–562, 1975.

Palmisano, A. C., J. B. SooHoo, R. L. Moe, and C. W. Sullivan, Sea ice microbial communities, VII, Changes in under-ice spectral irradiance during the development of Antarctic sea ice microalgae communities, *Mar. Ecol. Prog. Ser.*, *35*, 165–173, 1987.

Perovich, D. K., Seasonal changes in sea ice optical properties during fall freeze-up, *Cold Reg. Sci. Technol.*, *19*, 261–273, 1991.

Perovich, D. K., Light reflection from sea ice during the onset of melt, *J. Geophys. Res.*, *99*, 3351–3359, 1994.

Perovich, D. K., and J. W. Govoni, Absorption coefficients of ice from 250 to 400 nm, *Geophys. Res. Lett.*, *8*, 1233–1235, 1991.

Perovich, D. K., and A. J. Gow, A quantitative description of sea ice inclusions, *J. Geophys. Res.*, *101*, 18,327–18,343, 1996.

Perovich, D. K., and T. C. Grenfell, Laboratory studies of the optical properties of young sea ice, *J. Glaciol.*, *27*, 331–346, 1981.

Perovich, D. K., G. F. Cota, G. A. Maykut, and T. C. Grenfell, Bio-optical observations of first-year Arctic sea ice, *Geophys. Res. Lett.*, *20*, 1059–1062, 1993.

Pfirman, S., M. A. Lange, I. Wollenburg, and P. Schlosser, Sea ice characteristics and the role of sediment inclusions in deep-sea deposition: Arctic-Antarctic comparisons, in *Geological History of the Polar Oceans: Arctic Versus Antarctic*, edited by U. Bleil and J. Theide, pp. 187–211, 1990.

Reimnitz, E., E. W. Kempema, and P. W. Barnes, Anchor ice, seabed freezing, and sediment dynamics in shallow arctic seas, *J. Geophys. Res.*, *92*, 14,671–14,678, 1987.

Reimnitz, E., E. W. Kempema, W. S. Wever, J. R. Clayton, and J. R. Payne, Suspended-matter scavenging by rising frazil ice, in *Proceedings of the W. F. Weeks Symposium on Sea Ice Properties and Processes*, edited by S. F. Ackley and W. F. Weeks, *CRREL Monogr. 90-1*, pp. 97–100, 1990.

Roesler, C. S., and R. Iturriaga, Absorption properties of marine-derived material in Arctic sea ice, in *Ocean Optics 12*, edited by J. S. Jaffe, *Proc. SPIE Int. Soc. Opt. Eng.*, *2258*, 933–943, 1994.

Roesler, C. S., and M. J. Perry, In situ phytoplankton absorption, fluorescence emission, and particulate backscattering spectra determined from reflectance, *J. Geophys. Res.*, *100*, 13,279–13,294, 1995.

Shokr, M. E., and N. K. Sinha, Arctic sea ice microstructure observations relevant to microwave scattering, *Arctic*, *47*, 265–279, 1994.

Smith, R. C., Ozone, middle ultraviolet radiation and the aquatic environment, *Photochem. Photobiol.*, *50*, 459–468, 1989.

Smith, R. C., and K. S. Baker, Optical properties of the clearest natural waters (200–800 nm), *Appl. Opt.*, *20*, 177–184, 1981.

Smith, R. C., et al., Ozone depletion: Ultraviolet radiation and phytoplankton biology in Antarctic waters, *Science*, *255*, 952–959, 1992.

SooHoo, J. B., A. C. Palmisano, S. T. Kottmeier, M. P. Lizotte, S. L. SooHoo, and C. W. Sullivan, Spectral light absorption and quantum yield of photosynthesis in the sea ice microalgae and a bloom of *Phaeocystis pouchetti* from McMurdo Sound, Antarctica, *Mar. Ecol. Prog. Ser.*, *39*, 175–189, 1987.

Tucker, W. B., III, A. J. Gow, and W. F. Weeks, Physical properties of summer sea ice in the Fram Strait, *J. Geophys. Res.*, *92*, 6787–6803, 1987.

Weeks, W. F., and S. F. Ackley, *The Growth, Structure, and Properties of Sea Ice*, *CRREL Monogr. 82-1*, 130 pp., U.S. Army Cold Reg. Res. and Eng. Lab., Hanover, N. H., 1982.

Weeks, W. F., and A. J. Gow, Preferred crystal orientations along the margins of the Arctic Ocean, *J. Geophys. Res.*, *84*, 5105–5121, 1978.

Zeebe, R. E., H. Eiken, D. H. Robinson, D. Wolf-Gladrow, and G. S. Dieckmann, Modeling the heating and melting rate of sea ice through light absorption by microalgae, *J. Geophys. Res.*, *101*, 1163–1181, 1996.

W. S. Pegau, College of Oceanic and Atmospheric Sciences, Ocean Administration Building 104, Oregon State University, Corvallis, OR 97331.

D. K. Perovich, U.S. Army Cold Regions Research and Engineering Laboratory, 72 Lyme Road, Hanover, NH 07355. (e-mail: perovich@hanover-crrel.army.mil)

C. S. Roesler, Department of Marine Sciences, University of Connecticut, 1084 Shennecossett Road, Groton, CT 06340.

(Received July 8, 1996; revised April 18, 1997; accepted May 30, 1997.)